NE533 Fuel Performance MOOSE Project Writeup Part 1 + 2 + 3

TSU-CHUN TENG 200543795

Professor: Dr. Benjamin Beeler

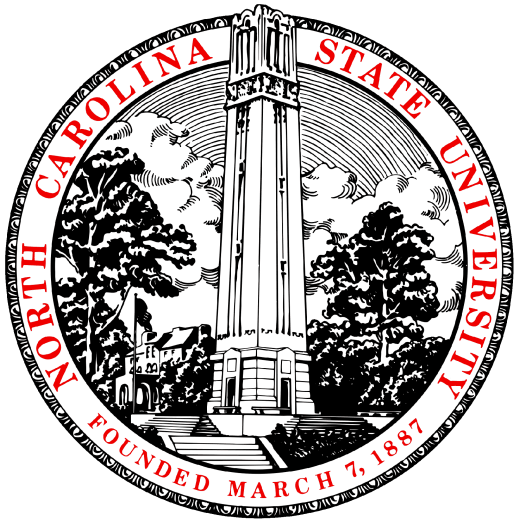

Department of Nuclear Engineering
North Carolina State University

April 26, 2024

Table of contents

Chapter 1

Introduction

In the NE533 Nuclear Fuel Performance course, we learned about numerous properties and calculations relevant to nuclear fuels, particularly for Light Water Reactors (LWRs). However, simply acquiring knowledge in class is insufficient; understanding its practical applications and utilizing simulation tools to solve real-world problems are crucial aspects. Therefore, the motivation behind this project is to deepen our comprehension of the key concepts covered in this course.

In Part 1, I developed the initial MOOSE input file and attempted to address the problem of monitoring the impact of fuel center-line temperature under both Steady and Transient States, considering constant thermal conductivity and temperature-dependent conductivity.

In Part 2, our focus shifts to examining the impact of introducing coolant into the system. Additionally, we utilized the "GapHeatTransfer" feature within the ThermalContact block (which can be seen as a type of boundary condition) to simulate the heat transferred across unmeshed gaps between two different blocks, rather than directly calculating it from our mesh.

In Part 3, our aim is to introduce coupled thermo-mechanical modeling into our system. We are attempting to observe the physical contact between the fuel pellet and cladding, and to investigate thermal expansion and irradiation swelling in our case.

Chapter 2

Methods

In this section, I will outline the important methods, key details, and parameters utilized in each part of this project.

2.1 Part 1

For Part 1, as outlined in Chapter 1, we will execute four distinct groups (Problems 1 to 4) in MOOSE:

1. Steady State w/ constant thermal conductivity k.
2. Steady State w/ temperature-dependent k.
3. Transient State w/ constant k.
4. Transient State w/ temperature-dependent k.

It's worth noting that the validity of the first group can be confirmed through comparison with the analytical solution taught in class.

2.1.1 The parameters, meshing methods, and other details

(i) The choices of materials and their parameters:

(A) *Fuel* $\rightarrow UO_2$: In steady state (the governing equation is

$$0 = \nabla \cdot (k \nabla T) + Q$$

When we consider the constant k, the thermal conductivity is $0.03\,\mathrm{W\,cm^{-1}\,K^{-1}}$ (From the lecture note); for the temperature-dependent k, the thermal conductivity (assuming the burnup FIMA=0) is

$$k_{\mathrm{ox}} = \frac{1}{A + B * T} = \frac{1}{3.8 + 0.0217 * T}$$

In transient state, we need more parameters for our governing equation is

$$\rho c_p (\frac{\partial T}{\partial t}) = \nabla \bullet (k \nabla T) + Q$$

Therefore, we take constant c_p=$0.33\,\mathrm{J\,g^{-1}\,K^{-1}}$, density=$10.97\,\mathrm{g\,cm^{-3}}$

(B) *Gap* $\rightarrow$ Pure He:

In steady state (the governing equation is

$$0 = \nabla \cdot (k \nabla T) + Q$$

When we consider the constant k, the thermal conductivity is $0.0025\,\mathrm{W\,cm^{-1}\,K^{-1}}$ (From the lecture note); for the temperature-dependent k, the thermal conductivity is

$$k_{\mathrm{He}} = 1.6 \times 10^{-5} \times T^{0.79}$$

But I also set if T<$600\,\mathrm{K}$(The assumption is made because we do not have a coolant system in Part 1. However, it's generally reasonable to set the initial condition for the temperature to be the coolant temperature.), k_{He}=$0.002\,556\,\mathrm{W\,cm^{-1}\,K}$ to avoid the error at t=$0\,\mathrm{s}$.

In transient state, take constant c_p=5.193 J g^{-1} K^{-1}, density=1.785 $\times$ 10^{-4}g cm^{-3}

(C) *Cladding* $\rightarrow$ *Zr*:

Assume the thermal conductivity of cladding is constant for our four problems, and the value is k_{He}=0.17 W cm^{-1} K (From the lecture note.) c_p=0.27 J g^{-1} K^{-1}, density=6.49 g cm^{-3}

(ii) Meshing:

Initially, I employed the GeneratedMeshGenerator to create the entire domain, while the SubdomainBoundingBoxGenerator was utilized to distinguish the fuel, gap, and cladding blocks. However, this mesh configuration posed potential issues for subsequent parts of the project. Consequently, I redefined the cladding first and separated the gap from the cladding, followed by separating the fuel from the gap. Initially, I set the number of meshes to 1000 and 100 in the x and y directions, respectively, for the entire domain. However, after considering the importance of mesh convergence testing, I determined that using 800 meshes in the x direction and 100 in the y direction provided the best fit for the analytical solution.

(iii) Others:

a The boundary condition on the right side is defined as a Dirichlet BC with a prescribed value for the temperature outside of the cladding, T_{co}=550 K. On the left side, the boundary condition is set as a Neumann BC, where the derivative of temperature normal to the boundary is zero.

b In many examples, PJFNK solvers were commonly used, but I often encountered divergent results when employing them. Eventually, I discovered that utilizing the NEWTON solver led to efficient and convergent outcomes.

2.2 Part 2

For Part 2, we will examine the impact of the flowing coolant on the heat removal from the fuel and its resultant temperature distribution. I initially maintained the same mesh design logic as in Part 1. Then, I adjusted some dimensions of the fuel pin to meet the given conditions outlined in Part 2.

2.2.1 The parameters, meshing methods, and other details

(i) The parameters:

The parameters, such as thermal conductivity, were derived from Part 1 steady state. However, for the sake of comparison with Part 3, I chose to make the thermal conductivity of the fuel temperature dependent. The mass flow rate of the coolant $\dot{m} = 0.25\,\mathrm{kg\,s^{-1}}$ rod, and the coolant specific heat $C_{PW} = 4200\,\mathrm{J\,kg^{-1}\,K^{-1}}$ (From the lecture note)

(ii) Meshing:

We basically utilize the mesh generated in part 1 but subsequently employ the BlockDeletionGenerator to remove mesh elements within the gap block after establishing the side sets of cladding-gap and gap-fuel.

(iii) Others:

(a) The boundary conditions on the side sets of cladding-gap and gap-fuel can be governed by the GapHeatTransfer function within the ThermalContact block.

(b) The Dirichlet BC we employed in Part 1 now becomes a function that varies with the length of the fuel rod. Meanwhile, the Neumann BC remains unchanged.

(c) In the original version of the Part 2 write-up, I directly equated the coolant temperature to the outer cladding temperature. This led to an underestimation of the temperatures of the outer cladding, inner cladding, fuel surface, and center-

line of the fuel. As a result, I modified the Dirichlet boundary condition and updated the results in section 3.2 by adapting the following equation.

$$T_{co} = T_{cool} + \frac{LHR}{2\pi R_{fuel} h_{cool}}$$

,where $h_{cool} = 2.65\,\mathrm{W\,cm^{-3}\,K^{-1}}$

2.3 Part 3

In Part 3, our objective is to utilize the Contact and Constrain module to observe displacement resulting from thermal and irradiation swelling. Additionally, we aim to investigate the possibility of detecting contact and interaction between the fuel and cladding. Initially, I maintained the same mesh design logic as in Part 2. Subsequently, I referenced an example from the MOOSE website and adjusted the method of defining the fuel pin to satisfy the specified conditions outlined in Part 3.

2.3.1 The parameters, meshing methods, and other details

(i) The parameters:

The parameters, including thermal conductivity, were obtained from Part 1 steady state results. I continue to utilize a temperature-dependent thermal conductivity for the fuel. Additionally, the mass flow rate of the coolant ($\dot{m}$) and the specific heat of the coolant (C_{PW}) are sourced from Part 2.

(ii) Meshing:

Initially, I employed the mesh generated in Part 2. However, I subsequently adopted a different approach to define the meshing by applying a method from the MOOSE website (`https://mooseframework.inl.gov/modules/combined/tutorials/introduction/step02.html`) and making some modifications to tailor it to our specific case. Initially,

I utilized the GeneratedMeshGenerator to define the separated blocks for the "fuel rod" and "cladding strip". By default, the "fuel rod" was assigned to block 1. Then, I used the SubdomainIDGenerator to designate the "cladding strip" as block 2. Finally, I employed the MeshCollectionGenerator to gather them together.

(iii) Others:

(a) The meshing strategy I employed simplifies the process of defining boundaries within the [BCs], [Contact], and [Constrain] blocks.

(b) In Part 2, the Dirichlet boundary conditions we utilized now have two versions: (1) Constant LHR (without axial variation) for the fuel heat source, and (2) Axially varying LHR. Meanwhile, the Neumann boundary condition remains unchanged.

(c) In addition to thermal swelling, I also considered the influence of irradiation (for gas and solid fission products) on swelling. However, I overlooked the densification effect.

(d) The parameters for irradiation swelling:

Assuming no densification, we only consider the strain from solid fission products and gas fission products, where $\Delta\rho_0 = 0.01$, β (burn-up) $= 9.87 \times 10^{-4}$, calculated as $\frac{\text{Fission Rate} \times \text{time}}{N_u}$, where Fission Rate $= 2 \times 10^{13}\,\text{fission}\,\text{cm}^{-3}\,\text{s}^{-1}$, time $= 2\,\text{weeks} = 1\,209\,600\,\text{s}$, and N_u (number density of U) $= 2.45 \times 10^{22}\,\text{U}\,\text{cm}^{-3}$. The density of UO_2 fuel is $10.97\,\text{g}\,\text{cm}^{-3}$. The results did not indicate any contact between the fuel and cladding, and I chose not to modify the thermal expansion coefficient of the materials. Instead, I extended the simulation time to 2 years ($63\,072\,000\,\text{s}$) and increased the burn-up to observe if any contact could be detected.

(e) Solving this part using steady-state methods proved to be less intuitive. Therefore, I opted to use the transient [Executioner] provided by the example and checked whether the solution reached to steady state or not. The result shows the Steady-State Solution Achieved at time: 39 (for both of the two sets)

Chapter 3

Results

3.1 Part 1

3.1.1 Analytical solution of steady state with constant k

Below is the calculation of the analytical solution:

Sol: As given, a steady state with constant k, LHR $= 350\,\mathrm{W\,cm^{-2}}$, $T_{co} = 550\,\mathrm{K}$, $R_f = R_{fuel}$ $= 0.5\,\mathrm{cm}$, $t_g = t_{gap} = 0.005\,\mathrm{cm}$, $t_c = t_{cladding} = 0.1\,\mathrm{cm}$

Take constant k, for fuel: $k_{fuel} = k_f = 0.03\,\mathrm{W\,cm^{-1}\,K}$, and for cladding: $k_{cladding} = k_c = 0.17\,\mathrm{W\,cm^{-1}\,K}$

$$\Delta T_c = T_{ci} - T_{co} = \frac{LHR}{2\pi R_f} \times \frac{t_c}{k_c} = \frac{350}{2\pi \times 0.5} \times \frac{0.1}{0.17} \approx 65.534\,\mathrm{K}$$

$$\Rightarrow T_{ci} = 550 + 65.534 = 615.534\,\mathrm{K}$$

The k for gap at $T = T_{ci} = 615.534\,\mathrm{K}$ is

$$k_{gap} = k_g = 16 \times 10^{-6} \times T^{0.79}\mathrm{W\,cm^{-1}\,K} = 2.556 \times 10^{-3}\mathrm{W\,cm^{-1}\,K}$$

$$\Delta T_g = T_s - T_{ci} = \frac{LHR}{2\pi R_f} \times \frac{t_g}{k_g} = \frac{350}{2\pi \times 0.5} \times \frac{0.005}{0.002556} \approx 217.935\,\mathrm{K}$$

$$\Rightarrow T_s = 615.534 + 217.935 = 833.469\,\mathrm{K}$$

$$\Delta T_0 = T_0 - T_s = \frac{LHR}{4\pi k_f} = \frac{350}{4\pi \times 0.03} \approx 928.404\,\mathrm{K}$$

$$\Rightarrow T_0 = 833.469 + 928.404 = 1761.873\,\mathrm{K}$$

3.1.2 MOOSE Results

The MOOSE simulation provided temperature profile results for problems (1) to (4), along with centerline temperature versus time data for problems (3) and (4). Table 3.1 presents the temperatures of the internal cladding, the surface of the fuel pellet, and the center of the fuel for each of these problems (1) to (4).

Table 3.1: The temperature data for the internal cladding, the surface of the fuel pellet, and the center of the fuel

Temperature (K)	Steady State Constant k		Steady State Temperature-dependent k	Transient State	
	Analytical	Numerical		Constant k	Temperature-dependent k
Centerline	1761.873	1766.5	1634.23	1071.37	922.139
Surface of the fuel pellet	833.469	839.091	833.904	673.899	671.985
Inner surface of cladding	615.534	609.509	609.509	575.312	575.311

The results displayed in Figure 3.1 to Figure 3.4 of the MOOSE simulation for the four groups were adjusted following modifications to their mesh definitions and subsequent attempts at mesh convergence testing.

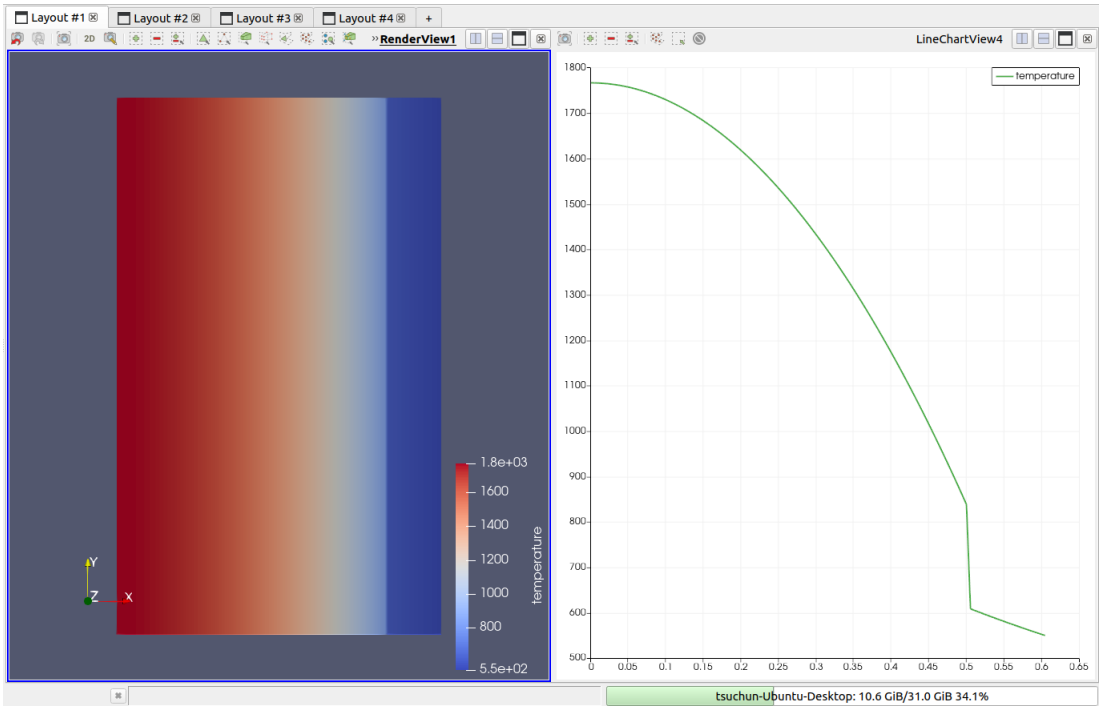

Figure 3.1: The temperature profile for Steady State Constant k (Problem (1))

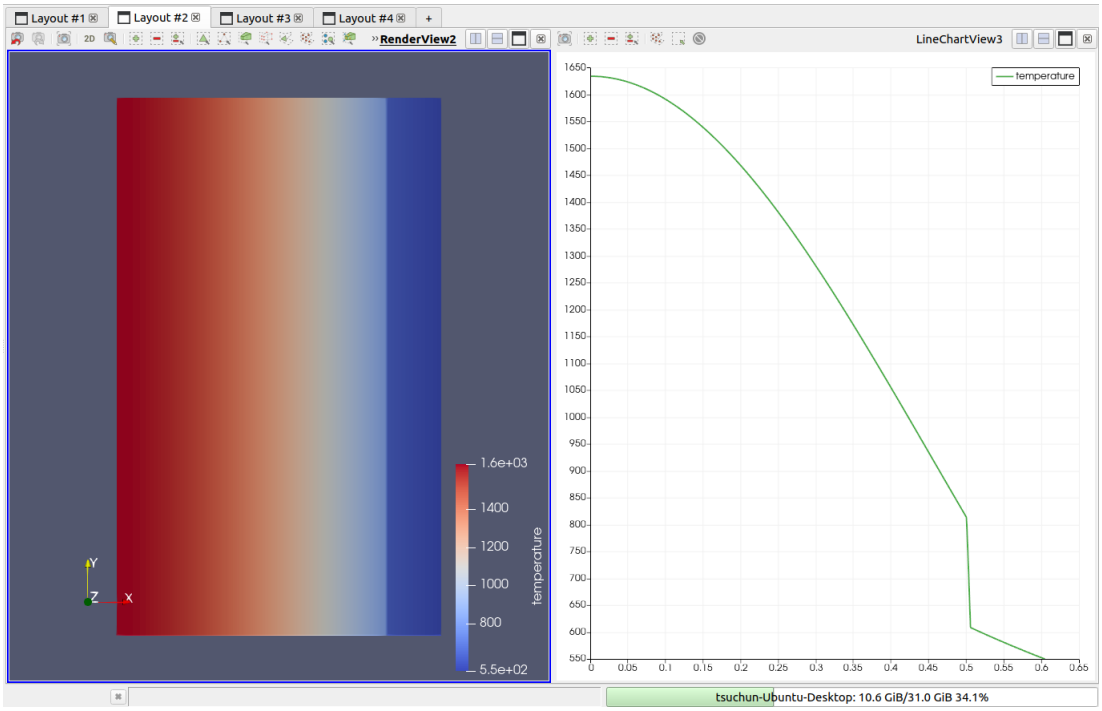

Figure 3.2: The temperature profile for Steady State Temperature-dependent k (Problem (2))

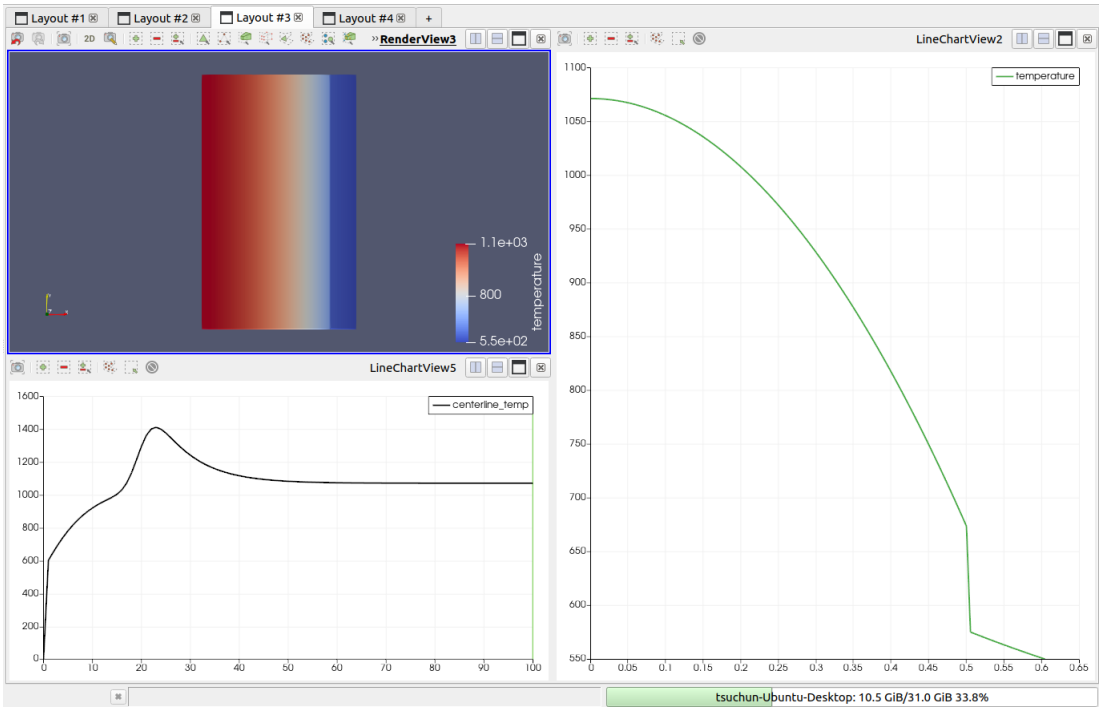

Figure 3.3: The temperature profile (Right) and the centerline temperature versus time (Lower Left) for Transient State Constant k (Problem (3))

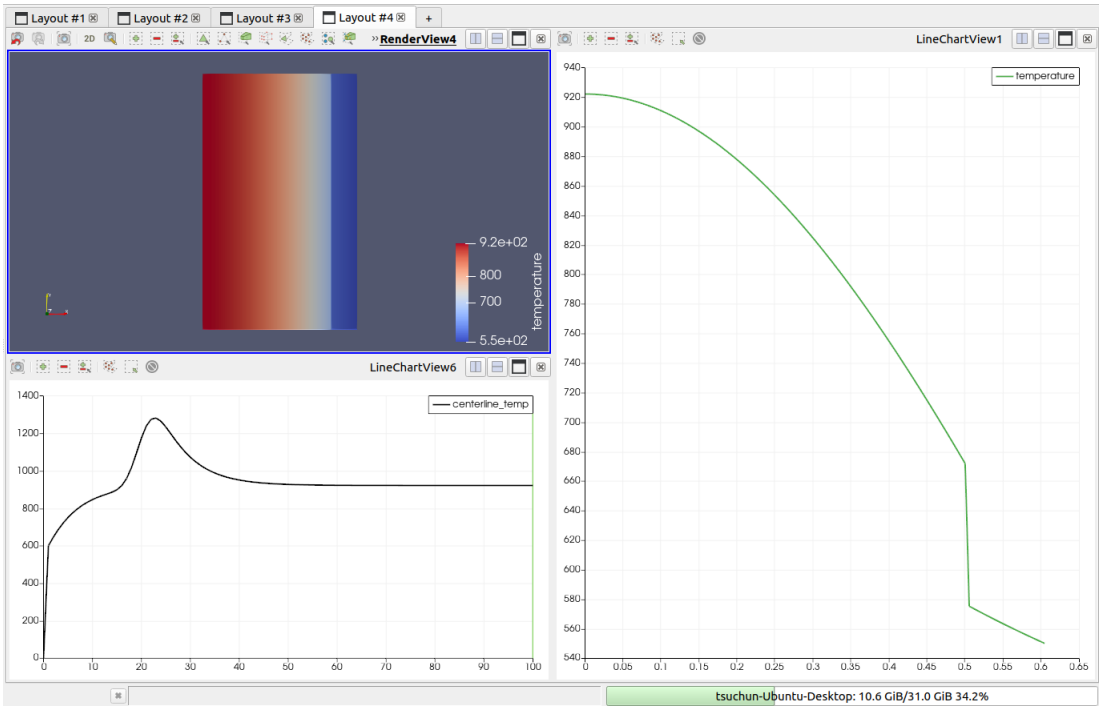

Figure 3.4: The temperature profile (Right) and the centerline temperature versus time (Lower Left) for Transient State Temperature-dependent k (Problem (4))

3.1.3 Discussion

Based on the results presented above, we can engage in a brief discussion regarding the outcomes through the following points.

(a) When comparing the analytical solution with the MOOSE results from group 1 in Part 1, it's evident that selecting the number of the division of $nx = 800$ and $ny = 100$ for the finite element mesh can yield a MOOSE solution with less than 1% error.

(b) In comparing these four groups, the crucial observation lies in whether thermal conductivity (k) is considered temperature-dependent or not. Notably, when we account for temperature dependency, significant changes in the center-line temperature are evident for both steady and transient states. However, the alterations in temperature on the surface of the fuel pellet and the inner surface of the cladding are relatively minimal.

(c) Overall, it's notable as well that the temperature profiles from the transient states are generally lower compared to those from the steady states.

3.2 Part 2

3.2.1 MOOSE Results

For the result of the temperature profile at three different heights on the fuel rod for the steady state with temperature-dependent k (only for fuel, the gap still maintains constant k.) by MOOSE are shown in Table 3.2, and from Figure 3.5 to 3.7. The center-line temperature distribution with the axis direction is presented in Figure 3.8

Table 3.2: The temperature profile at $z = 25$, 50, 100 cm

Temperature (K)	$z = 25$ cm	$z = 50$ cm	$z = 100$ cm
Centerline (T_0)	1414.29	1699.63	886.975
Surface of the fuel pellet (T_s)	792.904	851.432	676.381
Inner surface of cladding (T_{ci})	595.535	613.618	589.406
Outer surface of cladding (T_{co})	547.414	555.313	568.051
Coolant (T_{cool})	505.373	513.272	526.010

3.2.2 Discussion

(a) In Figure 3.5 to 3.7, the discontinuities in the temperature curves are noticeable. This occurs because we didn't directly solve for the temperature in the gap region using finite element mesh; instead, we utilized the ThermalContact method to address it.

(b) In Lecture 3, Dr. Beeler noted that in real-world scenarios, we should expect to observe a shift of the peak of the center-line temperature to around 60% to 65% of the rod's height. However, in Figure 3.8, we only observe a slight shift, approximately at 52% of the height. One potential explanation for this inconsistency could be linked to the fact that the actual length of the fuel pin typically extends to about 3 m, and in real-world scenarios, the mass flow rate tends to be slower. Consequently, as the coolant traverses

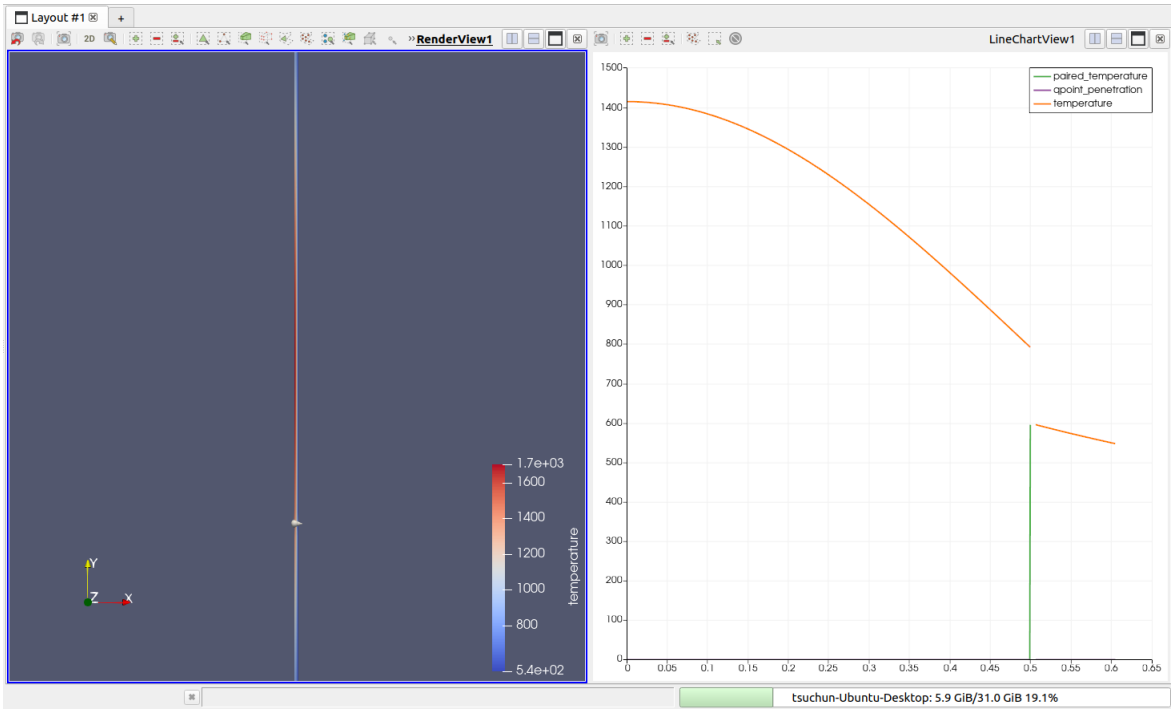

Figure 3.5: The temperature profile at the height z = 25 cm

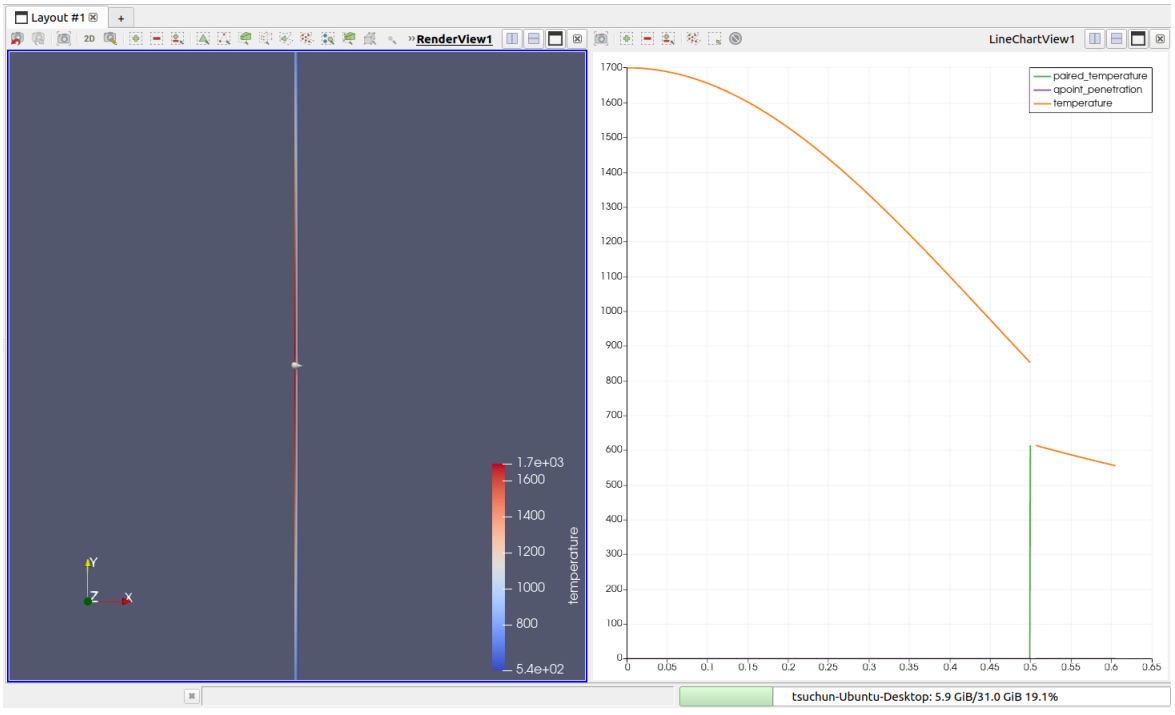

Figure 3.6: The temperature profile at the height z = 50 cm

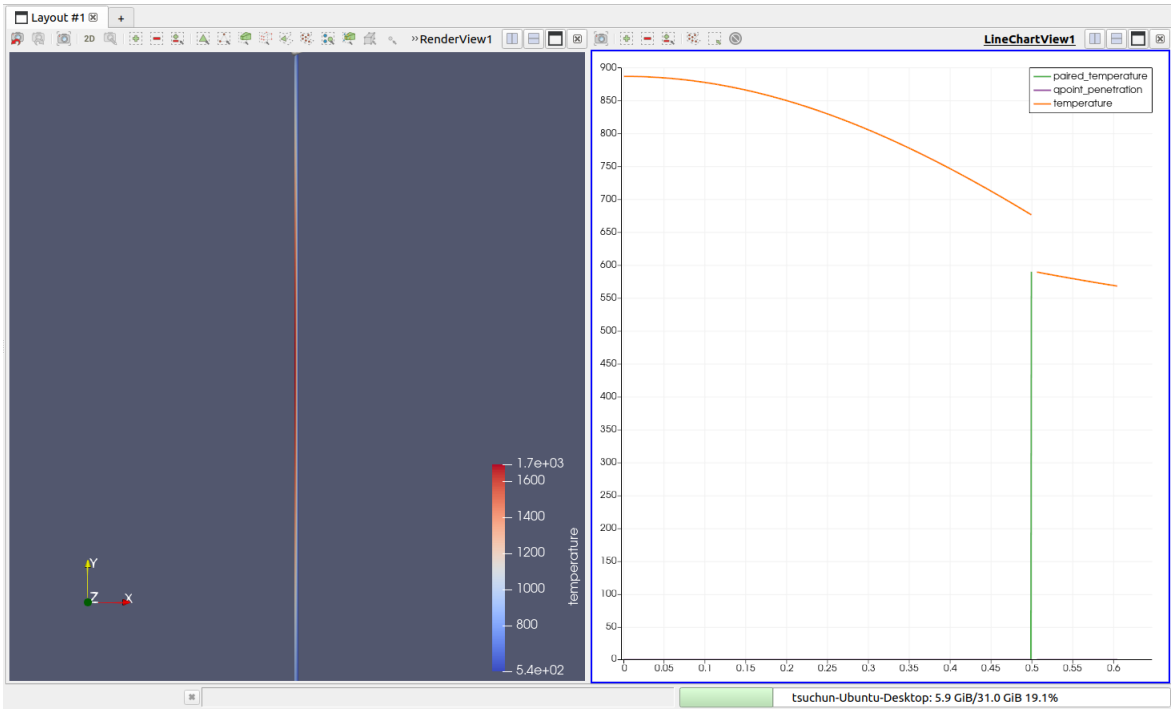

Figure 3.7: The temperature profile at the height z = 100 cm

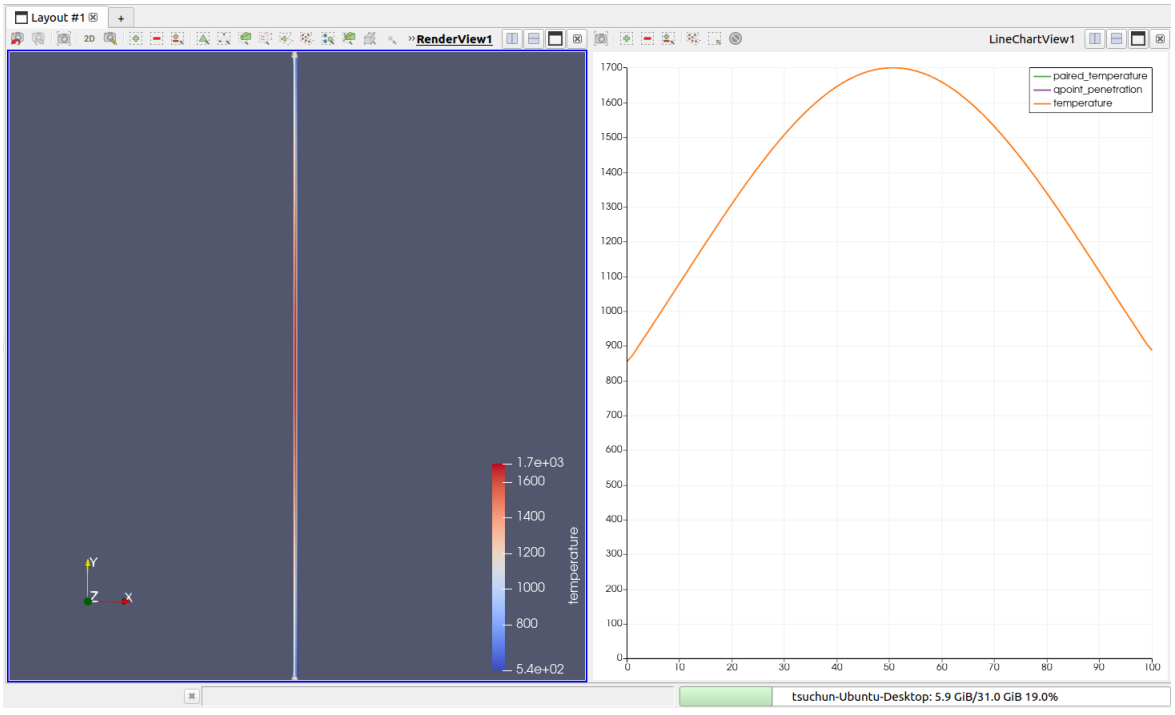

Figure 3.8: The center-line temperature in axial direction

upwards towards the upper part of the fuel, it may have a higher temperature, leading to a decrease in the efficiency of heat removal.

3.3 Part 3

In Part 3, I utilized parameters and information from the lecture notes, modifying some values while retaining others based on reasons to be discussed 3.3.2.

3.3.1 MOOSE Results

In this part, the provided results enable us to compare the effects and differences between axially varying LHR (Table 3.3 and Figure 3.9–3.16) and constant LHR (Table 3.4 and Figure 3.17–3.24).

Table 3.3: The temperature profile of the axially varying LHR set at $z = 25$, 50, 100 cm in the thermo-mechanical modeling

Temperature (K)	$z = 25$ cm	$z = 50$ cm	$z = 100$ cm
Centerline (T_0)	1191.64	1379.06	805.877
Surface of the fuel pellet (T_s)	656.793	677.59	610.247
Inner surface of cladding (T_{ci})	588.517	613.97	562.917
Outer surface of cladding (T_{co})	540.034	555.312	541.218

Table 3.4: The temperature profile of the constant LHR set at $z = 25$, 50, 100 cm in the thermo-mechanical modeling

Temperature (K)	$z = 25$ cm	$z = 50$ cm	$z = 100$ cm
Centerline (T_0)	1357.98	1370.26	1390.48
Surface of the fuel pellet (T_s)	665.338	673.496	683.696
Inner surface of cladding (T_{ci})	606.165	614.018	626.969
Outer surface of cladding (T_{co})	549.068	555.614	568.588

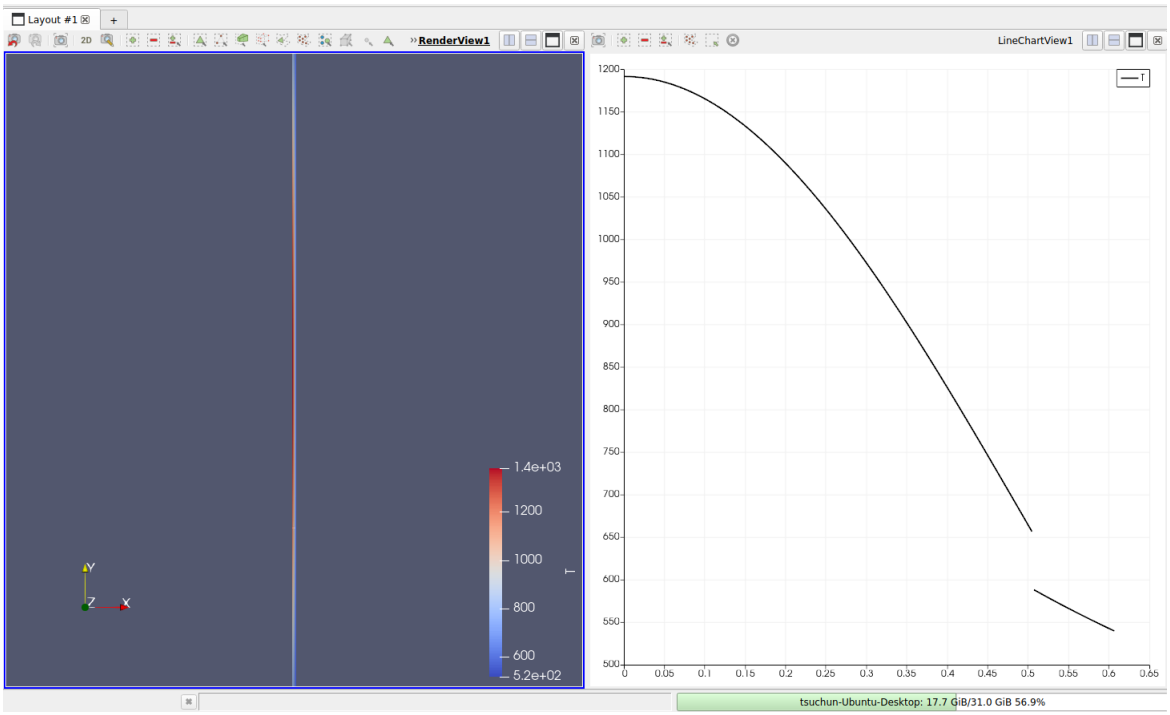

Figure 3.9: The temperature profile for axially varying LHR at the height z = 25 cm

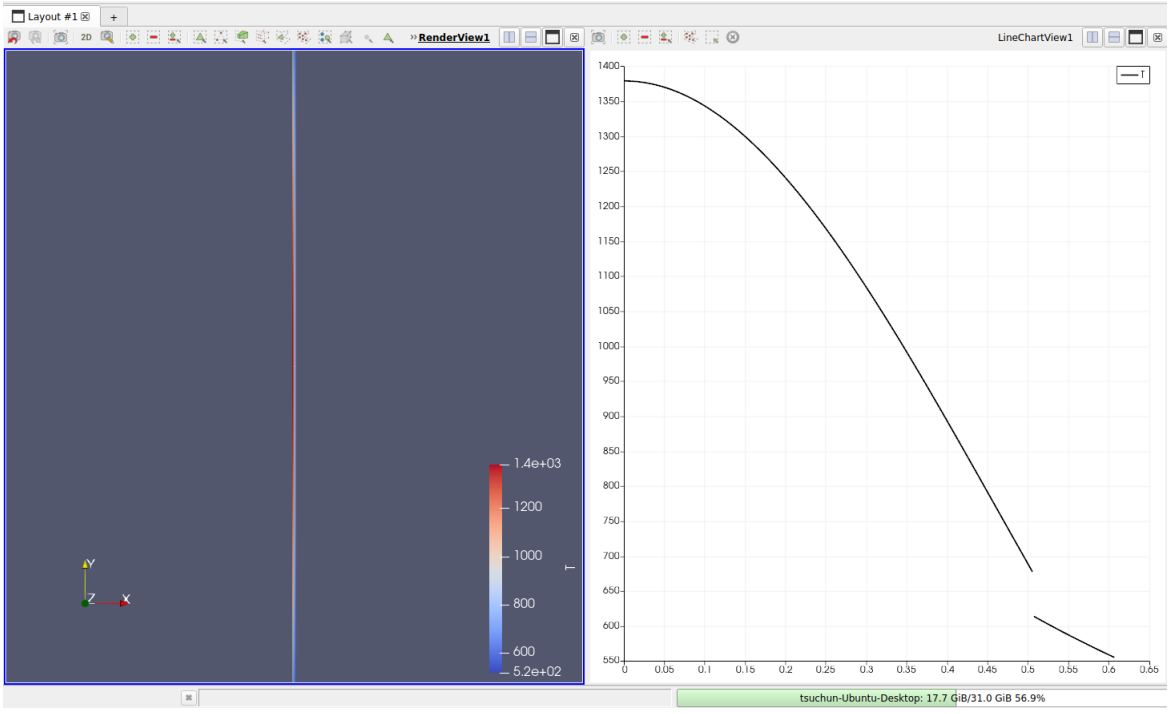

Figure 3.10: The temperature profile for axially varying LHR at the height z = 50 cm

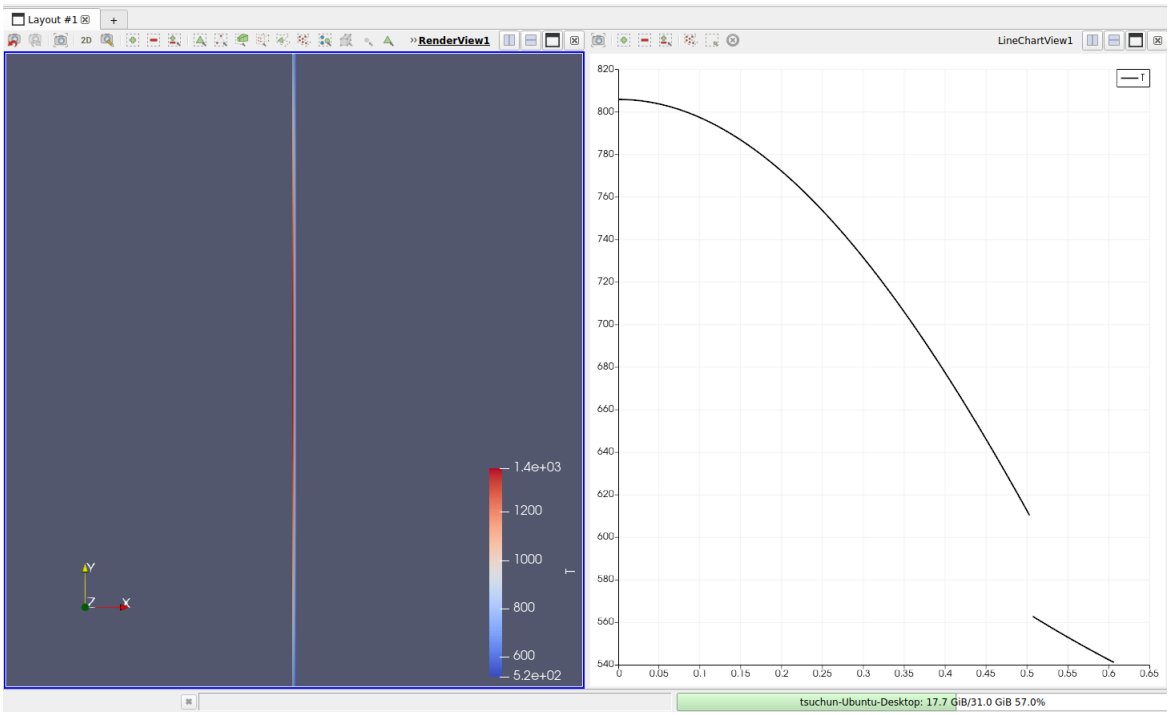

Figure 3.11: The temperature profile for axially varying LHR at the height z = 100 cm

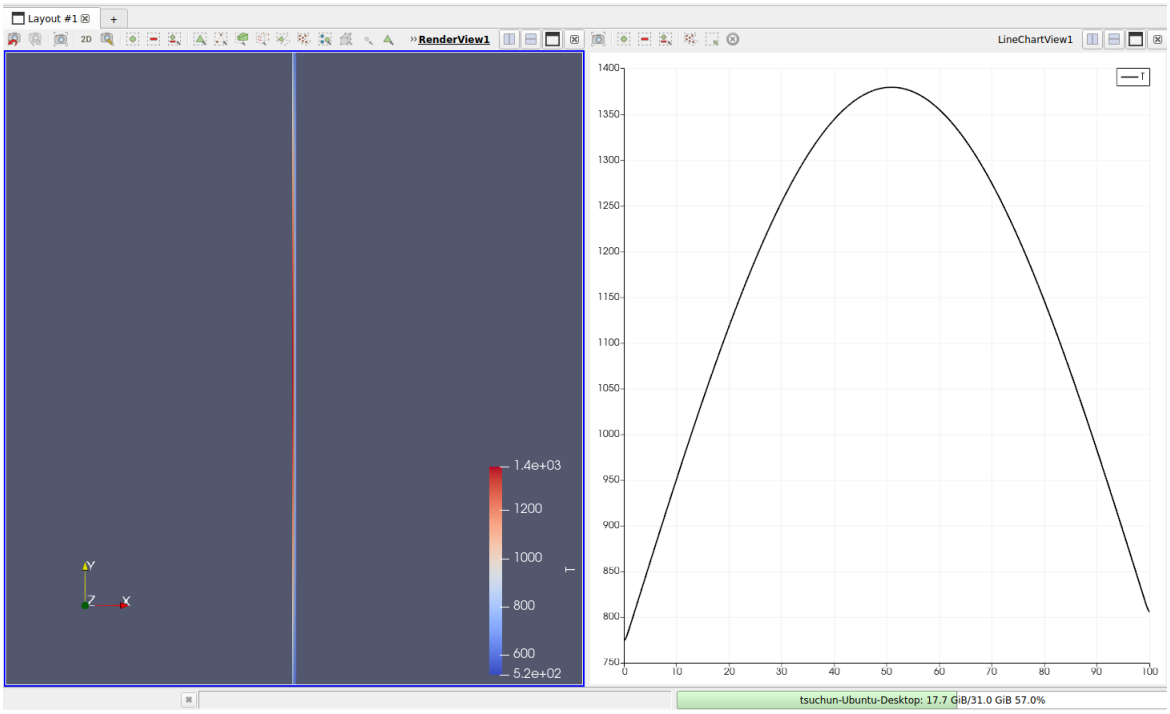

Figure 3.12: The center-line temperature set in the axial direction for axially varying LHR

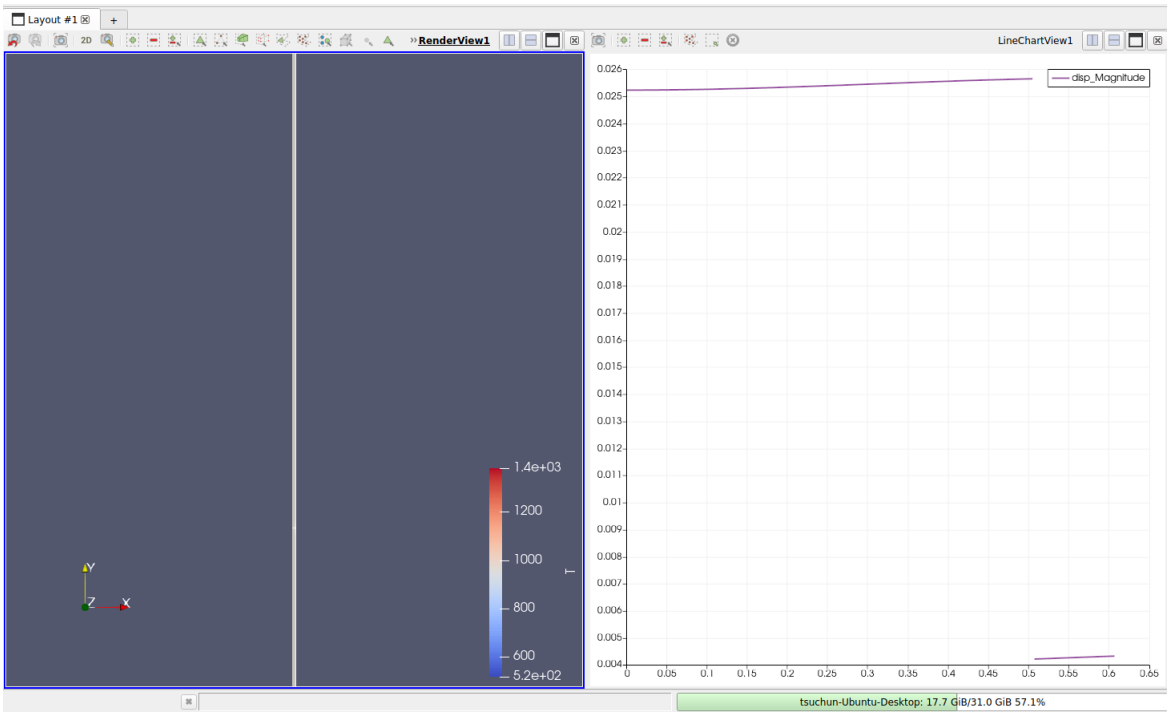

Figure 3.13: The displacement for axially varying LHR at the height z = 25 cm

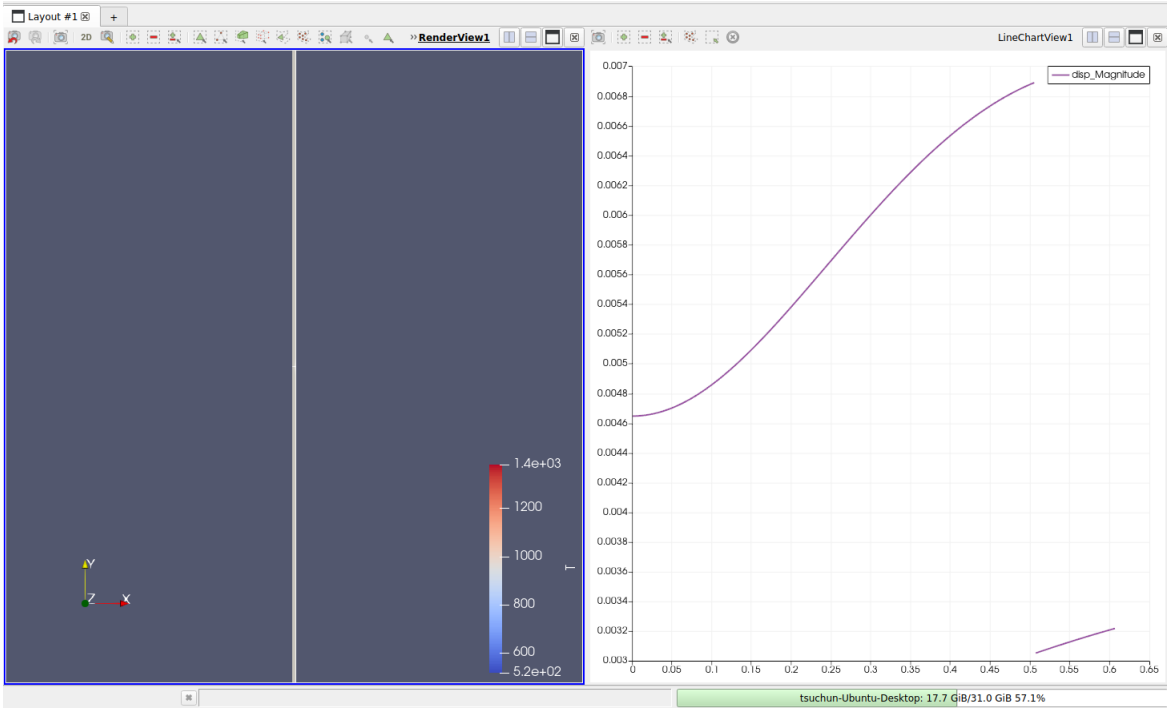

Figure 3.14: The displacement for axially varying LHR at the height z = 50 cm

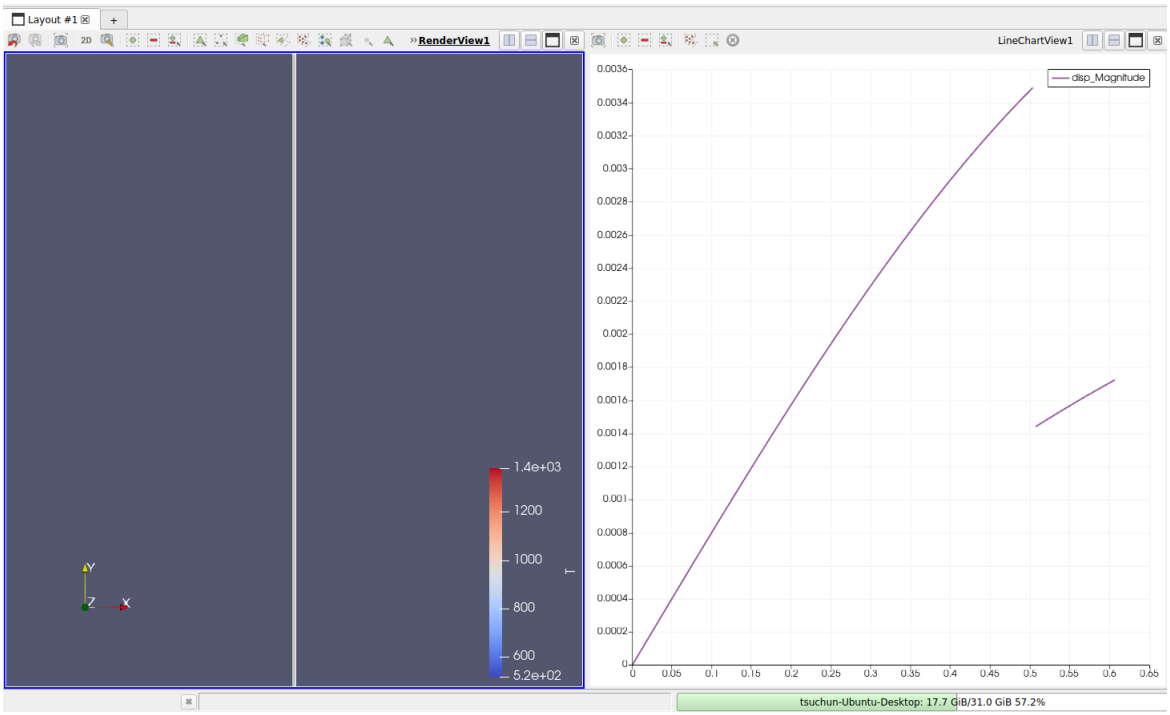

Figure 3.15: The displacement for axially varying LHR at the height z = 100 cm

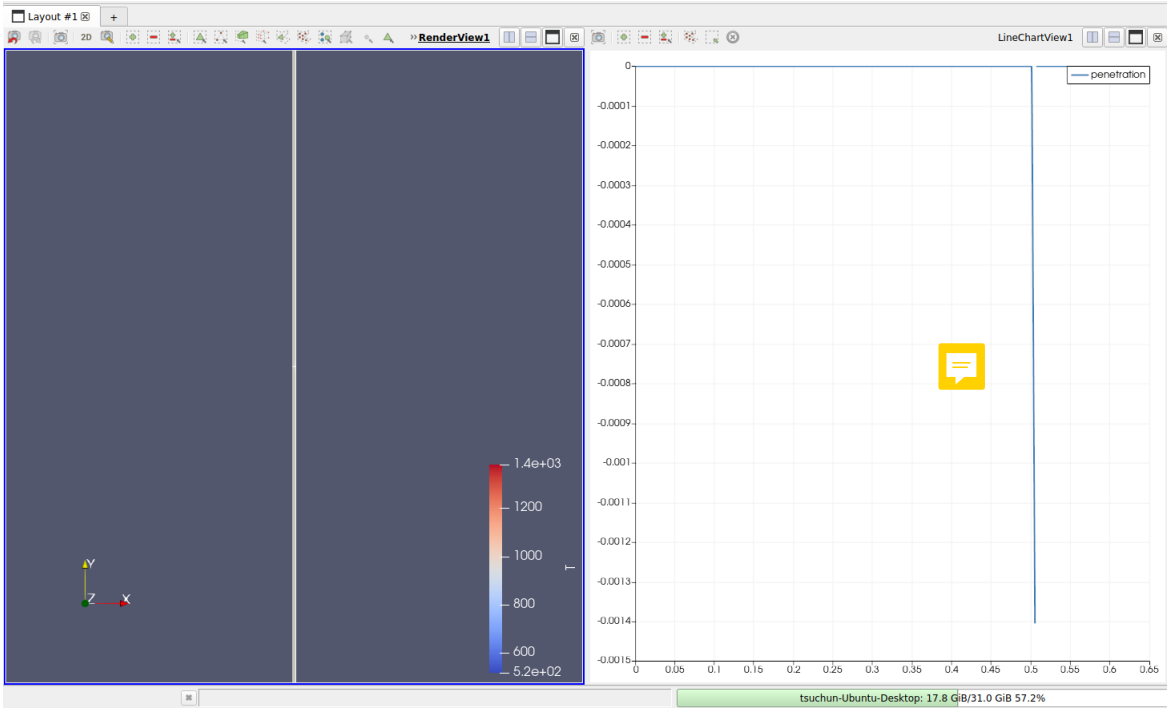

Figure 3.16: The penetration data for axially varying LHR at the height z = 50 cm

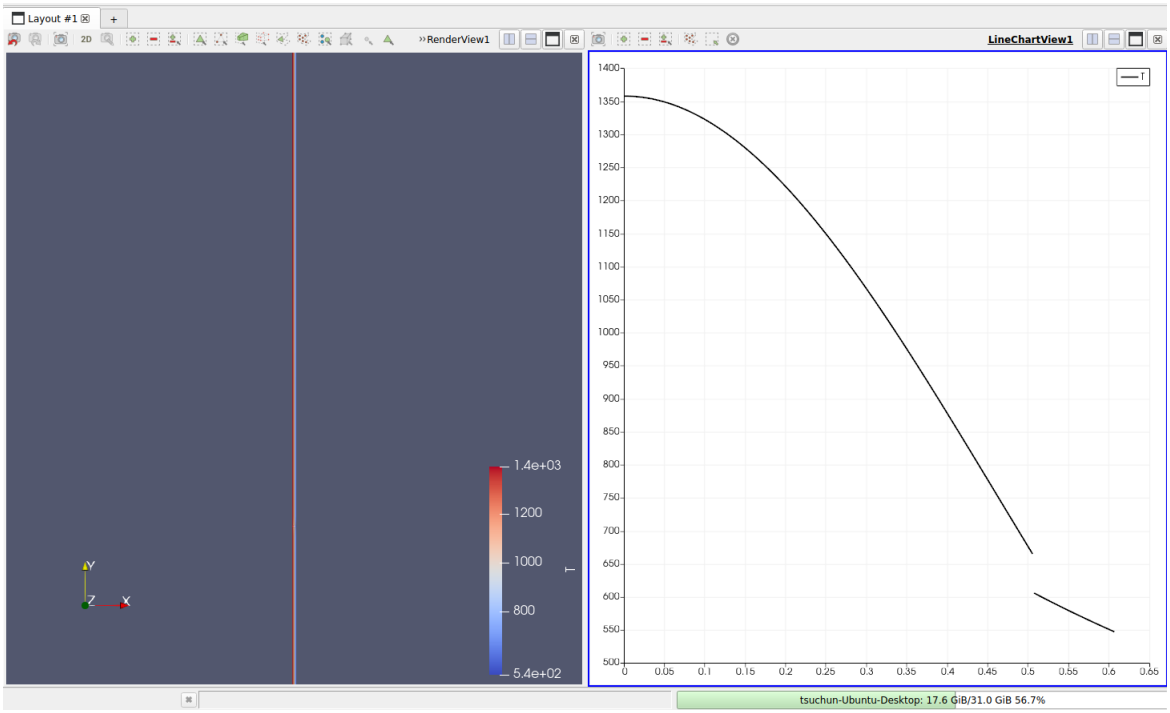

Figure 3.17: The temperature profile for constant LHR at the height z = 25 cm

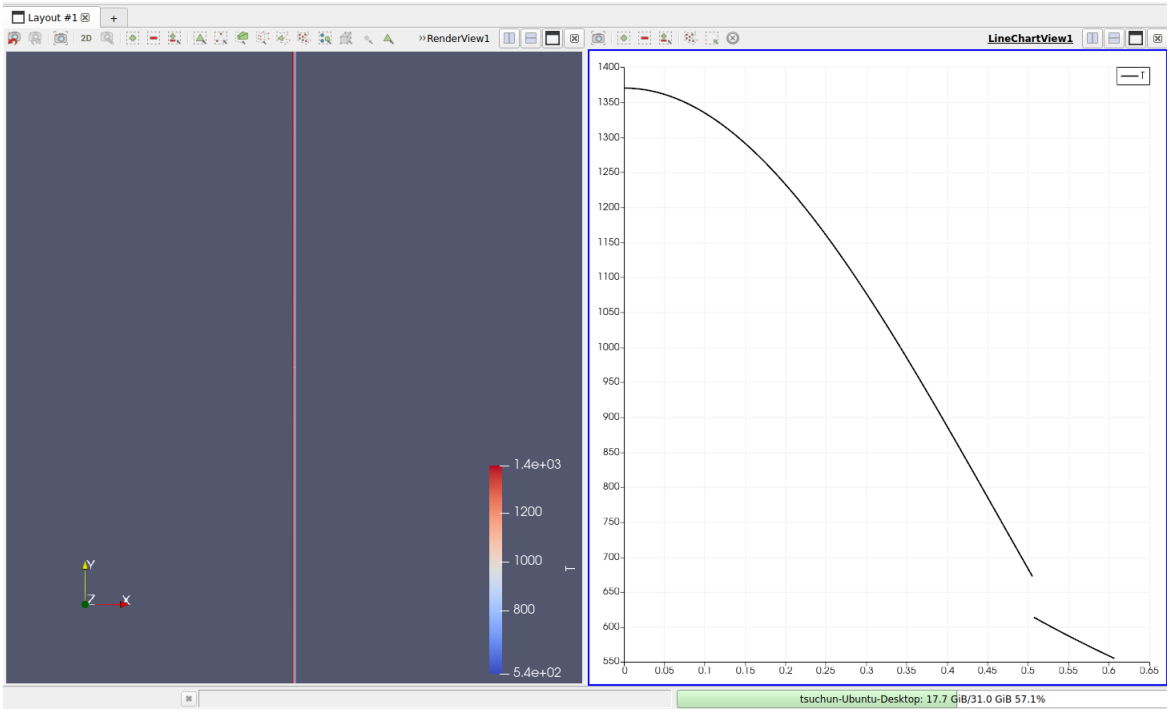

Figure 3.18: The temperature profile for constant LHR at the height z = 50 cm

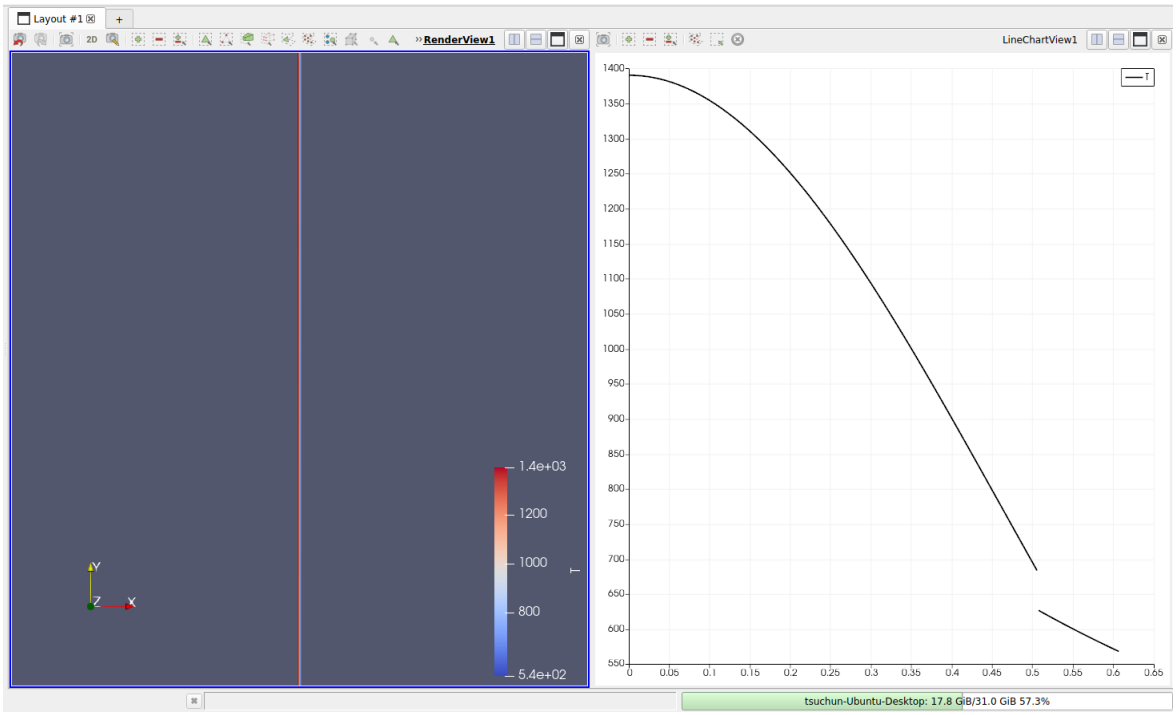

Figure 3.19: The temperature profile for constant LHR at the height z = 100 cm

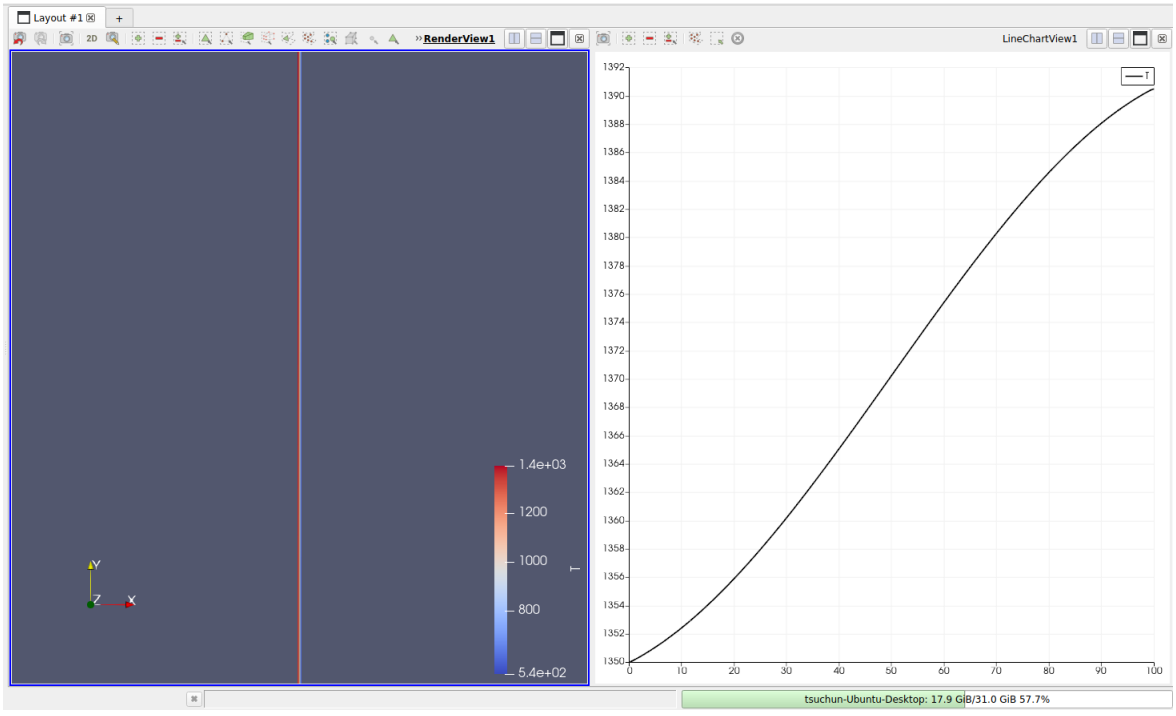

Figure 3.20: The center-line temperature set in the axial direction for constant LHR

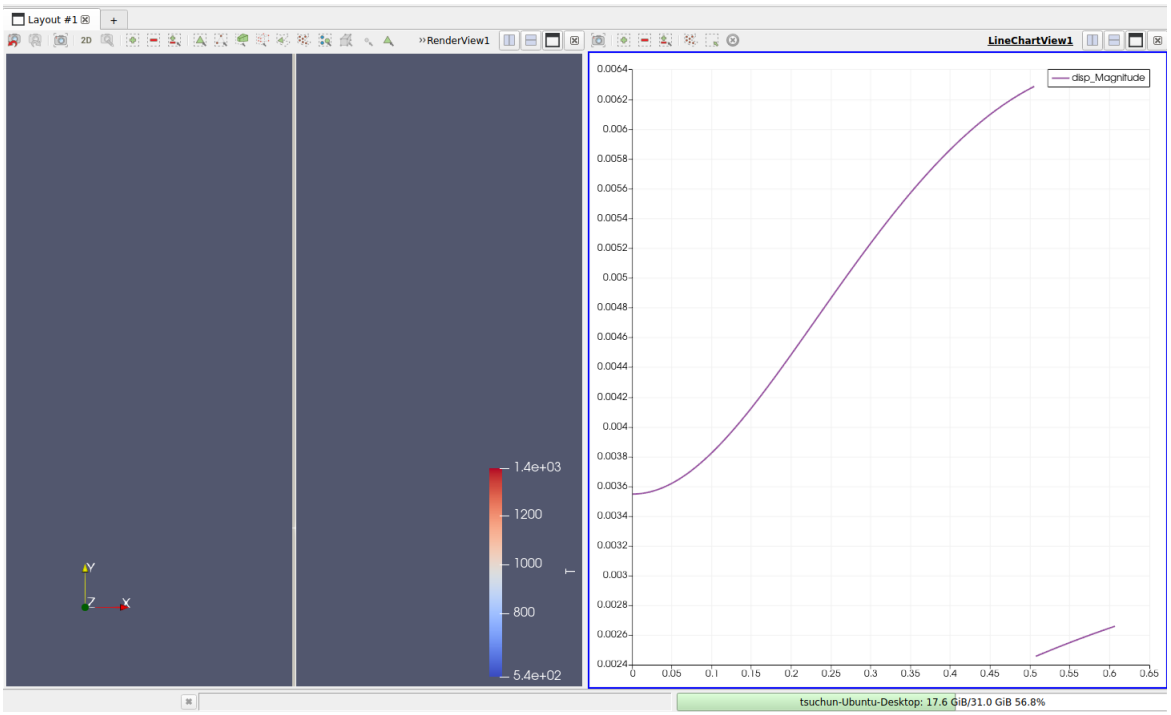

Figure 3.21: The displacement for constant LHR at the height z = 25 cm

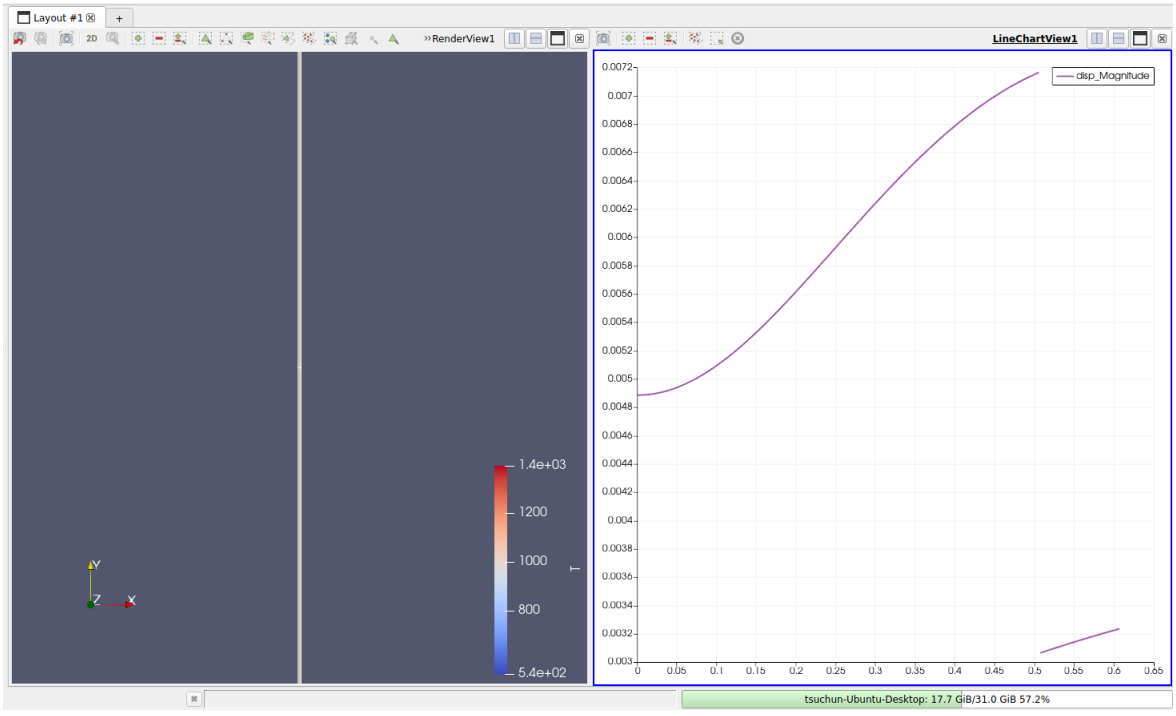

Figure 3.22: The displacement for constant LHR at the height z = 50 cm

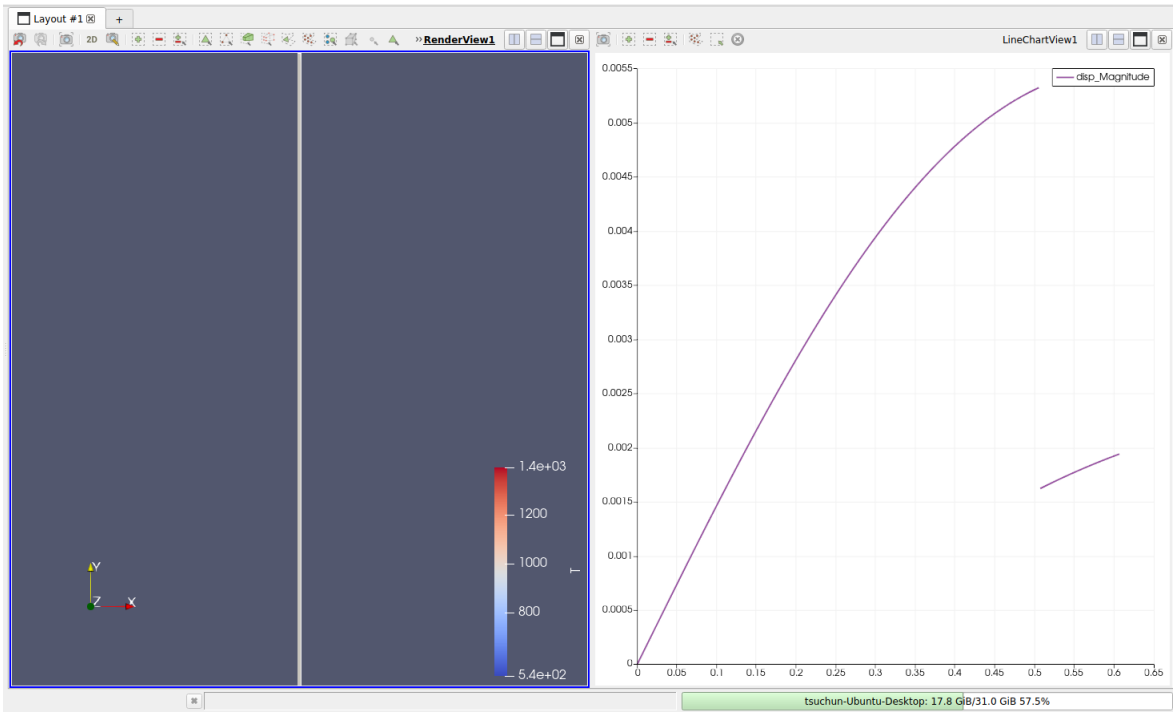

Figure 3.23: The displacement for constant LHR at the height z = 100 cm

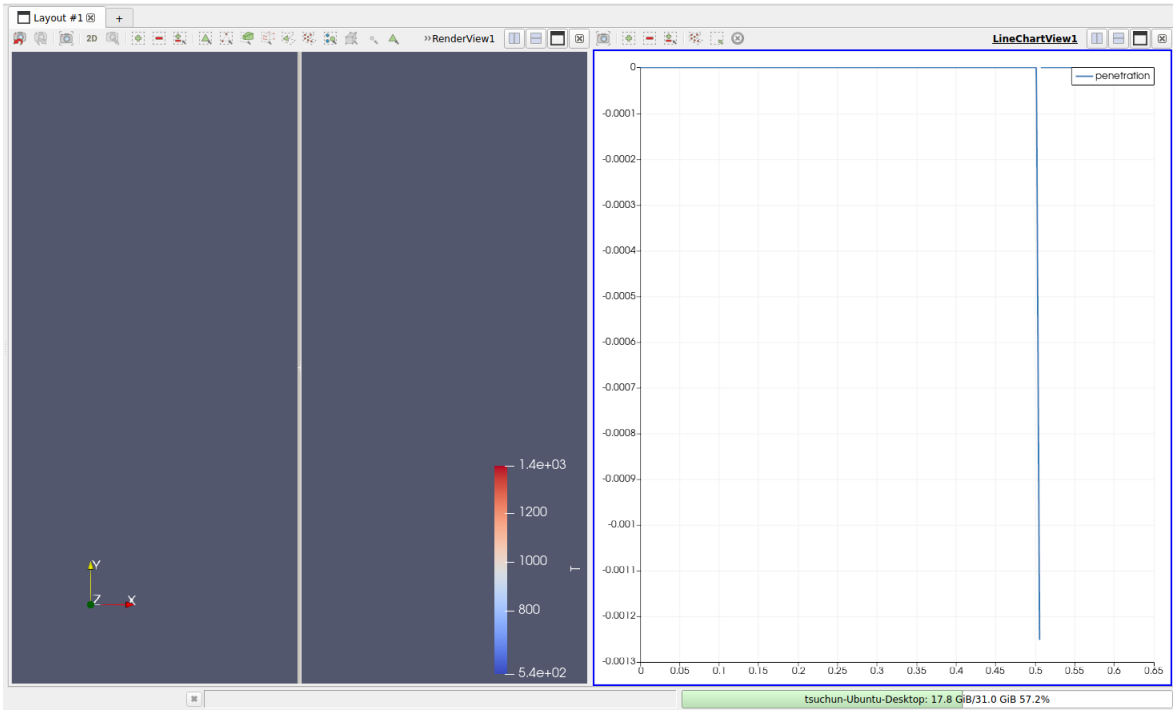

Figure 3.24: The penetration data for constant LHR at the height z = 50 cm

3.3.2 Discussion

(a) In Figure 3.9 to 3.11 and Figure 3.17 to 3.19, noticeable discontinuities can be observed in the temperature curves. This is because we didn't directly solve for the temperature in the gap region using a finite element mesh; instead, we utilized the Contact and Constraint method (as opposed to ThermalContact in Part 2) with a Lagrange multiplier (Tlm) for the temperature to address it.

(b) From Table 3.3 and 3.4, we can observe that the temperature for the constant LHR set is higher than that for the axially varying LHR set, especially for the part above the center of the fuel rod ($> 50\,\text{cm}$). The main reason is quite intuitive when we examine Figure 3.12 and 3.20.

(c) In the displacement results (Figure 3.13-3.15), the axially varying LHR set exhibits significantly higher values at $z = 25\,\text{cm}$. Conversely, for the constant LHR set (Figure 3.21-3.23), the values are similar, although the center displacement is slightly greater. The results indicate a similar trend for displacement, with larger values observed on the outer side for both the fuel and cladding. This could be attributed to the outer side having more free space to expand.

(d) As depicted in Figure 3.16 and 3.24, I did not observe any contact between the fuel and cladding. Upon analyzing the lack of observed contact, I identified two potential reasons: (1) The low burn-up time (2 weeks) in the example from Lecture 16, and (2) The dominance of thermal expansion, coupled with a small thermal expansion coefficient. For reason (1), despite attempting to increase the time to 2 years (resulting in significantly higher burn-up), the effect was not pronounced. As for reason (2), increasing the thermal expansion coefficient for the fuel from 11×10^{-6} to 11×10^{-5} and/or for the cladding from 7.1×10^{-6} to 7.1×10^{-5} resulted in non-convergence.

Chapter 4

Conclusion

This project has provided us with valuable insights into practical applications and has equipped us with the ability to utilize MOOSE for solving real-world problems. From this work, we can draw several key points.

(a) When comparing the analytical solution with the steady state results from MOOSE using constant thermal conductivity (k), it's possible to identify a mesh configuration that not only better approximates the analytical solution but also enhances the efficiency of the MOOSE simulation.

(b) Upon considering the temperature dependency of thermal conductivity, notable changes in the center-line temperature are observed for both steady and transient states. However, the variations in temperature on the surface of the fuel pellet and the inner surface of the cladding are relatively minor. Overall, it's worth noting that the temperature profiles from the transient states tend to be lower compared to those from the steady states.

(c) The discontinuities in the temperature curves are noticeable.(From Figure 3.5 to 3.7) This phenomenon arises from our decision not to directly solve for the temperature in the gap region using a finite element mesh. Instead, we opted to employ the Thermal-Contact method to handle this aspect.

(d) In real-world scenarios, we should anticipate a peak of the center-line temperature shifting much higher than the result we can observe in Figure 3.8. One potential explanation for this inconsistency could be attributed to the fact that the actual length of the fuel pin typically extends to about 3 m, and in real-world scenarios, the mass flow rate tends to be slower. Consequently, as the coolant traverses upwards towards the upper part of the fuel, it may have a higher temperature, resulting in a decrease in the efficiency of heat removal.

(e) The temperature is notably higher for the constant LHR set compared to the axially varying LHR set, particularly for the section above the center of the fuel rod. This observation becomes clearer upon reviewing Figure 3.12 and 3.20.

(f) The results suggest a consistent pattern in displacement, showing higher values on the outer side for both the fuel and cladding. This may be explained by the greater availability of space for expansion on the outer side.

(g) **Personal Reflection on this Project:**

This project posed a challenging learning curve for beginners in MOOSE, especially for Part 3 (Despite numerous discussions with Dr. Beeler, my classmates, and extensive research on the MOOSE website and fuel property papers, as well as trying various methods to solve the problem and achieve convergence, I still did not observe the PCMI in my results.) Despite the difficulty, I view it as an incredibly positive experience. Dividing the project into three parts was particularly helpful. It not only introduced us to a new tool but also encouraged us to improve our ability to search for resources that aid in our understanding. This skill development is invaluable for our career growth and future research endeavors.